# REDUCING THE UNCERTAINTY OF MULTI-WELL PETROPHYSICAL INTERPRETATION FROM WELL LOGS VIA MACHINE-LEARNING AND STATISTICAL MODELS

Wen Pan[1], wenpan@utexas.edu

Carlos Torres-Verdín[1,2], cverdin@austin.utexas.edu

Ian J. Duncan[2], ian.duncan@beg.utexas.edu

Michael J. Pyrcz[1,2], mpyrcz@austin.utexas.edu

[1] Hildebrand Department of Petroleum and Geosystems Engineering, The University of Texas at Austin, Austin, Texas, USA

[2] Bureau of Economic Geology, The University of Texas at Austin, Austin, Texas, USA

# Reducing the Uncertainty of Multi-Well Petrophysical Interpretation from Well Logs via Machine-Learning and Statistical Models

Wen Pan[1], Carlos Torres-Verdín[1,2], Ian J. Duncan[2], and Michael J. Pyrcz[1,2]

[1] Hildebrand Department of Petroleum and Geosystems Engineering, The University of Texas at Austin

[2] Bureau of Economic Geology, The University of Texas at Austin

## Abstract

Well-log interpretation provides *in situ* estimates of formation properties such as porosity, hydrocarbon pore volume, and permeability. Reservoir models based on well-log-derived formation properties deliver reserve-volume estimates, production forecasts, and help with decision making in reservoir development. However, due to measurement errors, variability of well logs due to multiple measurement vendors, different borehole tools, and non-uniform drilling/borehole conditions, conventional well-log interpretation methods may not yield accurate estimates of formation properties, especially in the context of multi-well interpretation. To improve the robustness of multi-well petrophysical interpretation, well-log normalization techniques such as two-point scaling and mean-variance normalization are commonly used to impose stationarity constraints for well logs requiring correction. However, these techniques are mostly based on the marginal distribution of well logs and require expert knowledge to be effectively implemented. To reduce the uncertainties and time associated with multi-well petrophysical interpretation, we develop the discriminative adversarial (DA) model and the linear constraint model for well-log normalization and interpretation. We also develop a new divergence-based type well identification method for improved test-well and training-well adaptation.

The DA neural network model developed for well-log normalization and interpretation can perform both linear and nonlinear well-log normalization by considering the joint distribution of all types of well logs and formation properties. To train the DA model, classical machine-learning models or classical petrophysical models are first trained to minimize the prediction error of formation properties in the training data set; then the adversarial model is trained to normalize well logs in the test set, such that the joint distribution of normalized well logs and formation property estimates of the test data set reproduce those of the training data set. The linear constraint model uses an ensemble of predictions from linear models to constrain both well-log normalization and interpretation. To identify wells with stationary formation properties as well as well logs, the divergence-based type well identification method is

developed to choose type wells for wells requiring correction based on well-log statistical similarity instead of closeness of wells.

We apply the developed methods to improve the accuracy of well-log normalization and the estimation of permeability in a carbonate reservoir. Six types of well logs and over 9000 feet of core measurements from 30 wells drilled between 1980s and 2010s in the Seminole San Andres Unit are available to validate the new multi-well interpretation workflow. Our interpretation models is flexible to integrate any types of classical machine-learning methods and petrophysical assumptions for robust petrophysical estimations. In comparison to classical machine-learning models with no normalization, with two-point scaling normalization and with linear constraints, the DA method yields better performance, e.g., the mean-squared error of permeability estimation decreases by approximately 20-50%. Our interpretation workflow can be applied to other stationary signal and image processing problems to mitigate errors introduced by biased measurements, and to better adapt models calibrated with data from one field to other neighboring fields.

## Introduction

Petrophysical interpretation is important for accurate reservoir characterization, reservoir modeling calibration and decision making during the reservoir development (Xu et al., 1992; Pan et al.,2021; Santos et al., 2021; Jo et al., 2021). However, the petrophysical interpretation of complex carbonate reservoirs, such as the prediction of formation properties, determination of geological settings and well-to-well correlation, is a major challenge in the oil and gas industry (Greder et al., 1996; Mohaghegh et al., 1997). Complexity of pore geometries, the role of micro fractures, and extensive modification of pore systems by diagenesis (Figure 1), confound the relationships and weaken correlations between various well logs, making prediction of formation properties, e.g., porosity, facies, and permeability with petrophysical models in carbonate reservoirs more challenging than for clastic sedimentary systems.
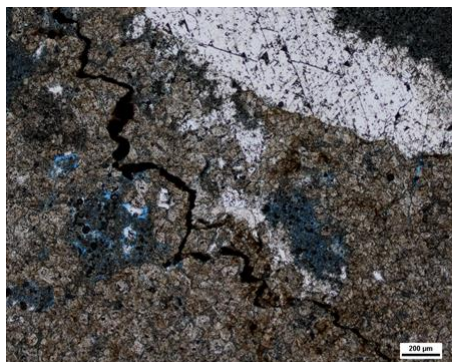


|        |        |        |
|--------|--------|--------|
| (A)    | (B)    | (C)    |
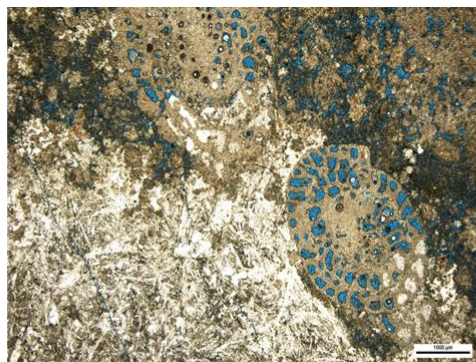
**Figure 1**. Optical microscope images and core images from cores at the Seminole San Andres Unit (SSAU), taken by Almirall (2019). Open Fractures at small (A) and large scales (C), filled and void pores (B) in carbonates make the accurate characterization of connectivity between pores difficult, resulting in a weaker correlation between porosity and permeability than for the case of sandstones, thereby posing formidable challenges for permeability estimation.

To perform more accurate reservoir characterization, many machine-learning methods have been previously proposed for lithology identification, depth matching, formation property estimation, and well-log correlation in carbonate and clastic reservoirs (Gashler, 2008; Bestagini et al., 2017; Sidahmed et al., 2017; Shashank and Mahapatra, 2018; Bennis and Torres-Verdín, 2019; Brazell et al., 2019; Liang et al., 2019; Shao et al., 2019; Yu et al., 2021). Compared to petrophysical model-based methods, e.g., Timur-Coats equation and Windland's equation (Leverett, 1941; Timur, 1968), machine-learning approaches obtain better results by fitting more complex relationships between well logs and formation properties. Common machine-learning methods used for well-log interpretation include random forest, feed-forward neural network, and convolutional neural network (CNN) (Collobert and Weston, 2008; Bhattacharya and Mishra., 2018; Zhu et al., 2018; Zhong et al., 2019). However, in almost all previous research, the training data set is formed by lumping data from all available wells and is not adapted to the test set, which implicitly assumes that the measurement error of well logs is stationary, i.e., the statistics of the error do not vary with well locations or depths, and the well-log interpretation is unique, i.e., formation properties can be uniquely determined from a set of well logs. However, these assumptions are not always valid in practice.

Uncertainties associated with environmental conditions introduced by different logging tools, vendors and vintage, and borehole fluids vary with wells and are not stationary, hampering effective multi-well petrophysical interpretation for carbonate reservoirs (Prasad et al., 2004). These uncertainties are exacerbated by the complexity of the borehole environment, as well as the behavior of drilling tools, typically alternatingly slippery and sticking, introducing errors that vary with well location and depth along the well. Furthermore, well-log interpretation is commonly non-unique because of incomplete or inadequate measurements, whereby different formation properties may yield similar well logs. Core measurements and well logs have different volumes of support and sampling rates, which also introduce uncertainties into well-based estimations (Mallan et al., 2018; Gaillot et al., 2019).

To reduce uncertainties associated with well logs and perform robust petrophysical interpretation, the assumption of stationarity of formation properties is commonly applied to constrain the interpretation. Well logs are normalized to be comparable to those of wells with the more accurate interpretation or core measurements. Normalization is the process of re-

scaling or re-calibrating the well logs so that they are consistent with the well logs acquired in other wells within the same field or region (Shier, 2004). Wells with interpreted well logs, calibrated with core measurements and corrected for borehole environmental effects, are denoted as *type wells* or *training wells*, and their well logs are denoted as *type well logs* or *training well logs*, respectively, while wells with well logs that require normalization and interpretation are denoted as *test wells*, and their well logs are denoted as *test well logs.* Normalization of test well logs reduces errors introduced by variations in environmental and measurement conditions and non-uniqueness by adapting test wells to type wells, thereby making models calibrated with type wells robust for test well-log interpretation.

Imposing constraints to petrophysical interpretation based on the stationarity assumption of formation properties and well logs is an important aspect in petrophysics that has not been well-studied. In conventional normalization methods, e.g., two-point scaling methods (Shier, 2004), one first identifies type wells with formation properties that are regionally or globally representative. Then, each test well log is linearly normalized to have values for two formations with distinct formation properties that are the same as those of type wells, e.g., the gamma-ray log values of pure shale and sandstone facies in a test well are normalized to be the same as those of type wells. The values for distinct formation properties are usually chosen as the minimum and maximum values within an interval (Shier, 2004). When formation properties are stationary among test and type wells, test well logs exhibit marginal distributions similar to those of the type wells. The marginal distribution of a well log is its histogram. This normalization method is also known as affine correction in geostatistics (Pyrcz and Deutsch, 2014). According to Shier (2004), there are 5 common methods for type well identification. Based on their assumptions of stationarity, they can be roughly divided into two categories (Figure 2):

1). **Stationary reservoir assumption**: the specified statistics of well logs are invariant over a specified interval (Figure 2A). The big histogram well-log normalization method (Shier, 2004) makes this assumption. In the big histogram method, one normalizes test well logs to match those from all type well logs in the field. We refer to this category of methods as the *stationary well method*.

2). **Non-stationary reservoir (regional stationarity) assumption**: the specified statistics of well logs are variant over a specified interval (Figure 2B). The non-stationarity of well logs is introduced by non-stationary formation properties trends or different logging environments. Type well, neighbor comparisons, and the trial normalization method (Shier, 2004) make this assumption. For the latter methods, one normalizes test well logs to match the nearest type well log(s). We refer to this category of methods as the *type well method*.
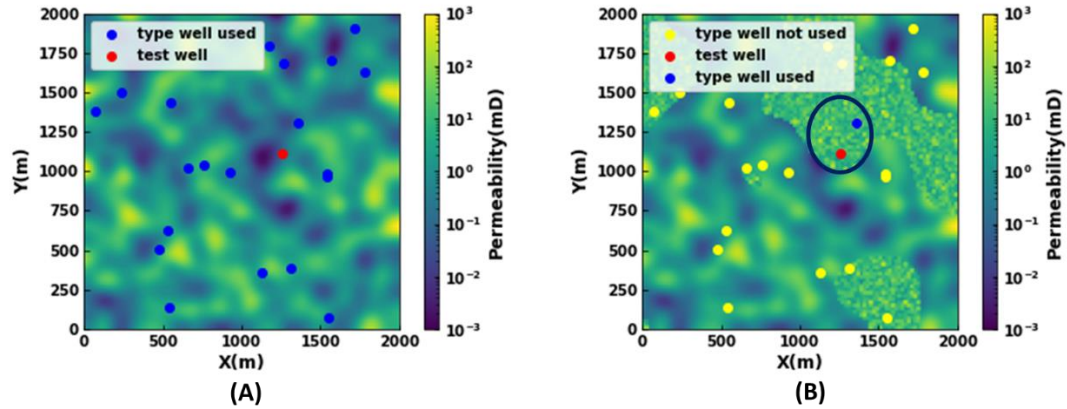
**Figure 2**. Well-log normalization methods based on different assumptions. (A) In a stationary reservoir, the statistics of well logs from a test well are normalized to match those from all type wells. (B) In a non-stationary reservoir, the statistics of well logs from a test well are normalized to match those of nearby type well(s).

There are three limitations in classical well-log normalization methods: (1) the successful application of the normalization depends heavily on the experience of the interpreter; a bad choice of normalization parameters, such as the two points representing different facies in the two-point scaling method (Shier, 2004), or a bad choice of type wells can introduce bias into the interpretation results, such as over alignment. Over alignment is the situation where the statistics of formation properties from one well are different from those of the type wells, whereas well logs are incorrectly normalized to exhibit the same distribution. (2) Conventional normalization methods only normalize test well logs to reproduce the marginal distribution of each individual type well log, i.e., the histograms of each well log. However, the reproduction of marginal distributions does not guarantee a reproduction of correct correlations between different types of normalized well logs; a misleading correlation between normalized well logs can degrade the performance of the interpretation models, whereby the joint distribution of the multiple well logs needs to be considered, where the joint distribution is the distribution of a well log given other types of well logs. (3) Conventional normalization methods are linear normalization methods. However, bias introduced by borehole environments can be nonlinear and varies with other formation properties, e.g., facies, resulting in non-linear structures that must be corrected with normalizing joint distributions.

To normalize well logs such that test well logs have joint distributions similar to those of type well logs, one can minimize the divergence between the joint distribution of type well logs and test well logs. Divergence measures, such as the Kullback–Leibler (KL) divergence (Kullback and Leibler, 1951) and Jason-Shannon (JS) divergence (Manning and Schutze, 1999), can be used to

quantify the statistical dissimilarity between two joint distributions. Chang et al. (2021) use the maximum mean discrepancy domain transfer (MMDDT) learning model to predict rock facies, which implicitly imposes the spatial stationarity assumption and minimizes the divergence for the outputs of intermediate layers in a neural network, i.e., the intermediate features, during training. The intermediate features are non-linear transformations of the input well logs, thus can also be regarded as non-linearly normalized well logs for corrected joint distributions. However, in their model, the prediction error and divergence are minimized simultaneously; differences in the convergence time of these two loss functions lead to either overfitting or over alignment in petrophysical interpretation. The model is not flexible enough to be applied with other pre-trained machine-learning or calibrated petrophysical models due to synchronized training. The output facies prediction is not constrained based on stationarity assumption. Furthermore, the lack of physical meaning for the intermediate features makes it difficult to interpret the results and provide useful findings.

To avoid the above limitations, we propose to use a modified asynchronized discriminative adversarial (DA) domain adaptation (Tzeng et al., 2017) to normalize and interpret well logs. In the modified DA model, the predictive layers, i.e., layers that map normalized well logs to formation properties, either continuous or categorical, are first trained. Then preprocessing layers are trained to normalize test well logs by minimizing the divergence between normalized test well logs and type well logs and associated predictions through a discriminator neural network. With this structure, the prediction error of formation properties and the Jason-Shannon divergence (JSD) are minimized asynchronously to avoid overfitting or over alignment. The predictive layers can be pre-trained petrophysical or machine-learning models, making the model more flexible and interpretable. Intermediate features in the DA model are normalized well logs that are comparable to training well logs from properly selected type wells, which are more interpretable.

With this model, we also mitigate the remaining two limitations of conventional well-log normalization methods, i.e., nonlinear normalization can be performed with nonlinear preprocessing layers, the divergence is calculated in the feature space identified by a discriminator neural network, which can avoid over alignment. Table 1 summarizes the salient properties of different normalization methods.

| Method | Loss | Calibration | Operation |
|---|---|---|---|
| Two-point scaling | univariate statistics | asynchronized | linear |
| MMDDT | MMD | synchronized | (non)linear |
| DA | JSD | asynchronized | (non)linear |

**Table 1**. Summary of the properties of different scaling methods used in well-log normalization.

Compared to previous methods, the asynchronized DA model we propose for multi-well petrophysical interpretation mitigates overfitting and over alignment problems, improves the accuracy and interpretability of well-log normalization, and provides more robustly decision making.

To apply the divergence-based well-log normalization, two assumptions need to be made: (1) well logs and core measurements from the type wells are of good quality and test wells and associated type wells exhibit similar formation properties. (2) Type wells exhaustively sample the formation penetrated by test wells, i.e., one can find at least one type well with formation property distribution similar to any of the test wells. When the type wells have biased samples compared to the test wells, data balancing and semi-supervised learning should be applied.

To make these two assumptions valid, proper selection of type well(s) for test well(s) is important. To choose the type well(s), we propose two divergence-based type well identification methods for stationary and non-stationary formation property distribution. These methods better capture the statistical similarities between training and test wells, compared to classical distance-based type well identification method, which only considers spatial distance and rely on spatial continuity of formation properties. Statistical similarity is a better metric to choose training wells that exhibit formation property statistics similar to those of a test well, especially in the case where formation properties are non-stationary among wells, e.g., adjacent wells may penetrate different zones.

# Method

In this section, we first describe the data used to compare our proposed methods to conventional methods for the case of permeability prediction, then we introduce the structure of the DA model for well-log normalization and permeability prediction. We use our proposed DA model to calculate normalized test well logs and associated permeability prediction that reproduce the joint distribution of type well logs and associated permeability measurements, mitigating errors introduced by non-stationary well logs. The DA model assumes stationary formation properties and well logs from the test well and associated type wells and adds constraints to improve the accuracy of the interpretation.

Another new model proposed here to perform the normalization and permeability prediction is the linear constraint model, which uses an ensemble of linear model predictions from the linear well-log interpretation model and the linear stationarity model to constrain the well-log normalization and interpretation instead of DA loss in a DA model. The DA, linear constraint, two-point scaling and unconstrained interpretation workflows are compared in the Results section of this paper to decide on the best interpretation workflow for well-log normalization and permeability prediction in the examined carbonate reservoir.

Divergence-based type well identification methods are also discussed in this section to address the problem of non-stationary formation properties among different wells and compared to the distance-based type well identification method in Results section.

Compared to conventional well-log normalization, type well identification and well-log interpretation models, we expect our new methods to perform more effectively for multi-well petrophysical interpretation, and to predict formation properties more accurately from well logs in the presence of environmental uncertainties, spatial continuity/discontinuity and (regional) stationarity.

## Data Preparation

Our proposed method is verified with core measurements and wireline log data from the Seminole San Andres Unit (SSAU), a dolomitized carbonate reservoir located on the eastern shelf of the Central Basin, West Texas, USA (Wang et al., 1998). The SSAU has produced more than 700 million barrels of oil from the upper and lower San Andres formations, with water flooding conducted between 1960 and 1980 and $CO_2$ flooding since the 1980s. Rock porosity in the producing reservoir zone ranges from 5% to 20%, while permeability ranges from 0.01 mD to 2000 mD (Male and Duncan, 2020). We select 30 wells with core measurements and complete well logs from 625 wells drilled between 1940 and 2010. The well logs used as inputs for permeability estimation are gamma-ray (GRD), density (RHOB), neutron porosity (NPHI) and compressional slowness (DT), along with relative depth and porosity estimates. The caliper log (CALD) is used for well-log quality control. Core porosity (CPOR) and maximum horizontal permeability (CKMAX) from cores are used to calibrate and validate our interpretation workflow (Figure 3).

Several steps are taken to perform the quality control: (1) Abnormal spikes and outliers in well logs are evaluated for potential errors; (2) caliper logs are used to identify intervals with severe borehole washouts; (3) well logs are depth shifted by matching the troughs and peaks of core porosities and the interpreted porosity log.

Wells are divided into the training set consisting of type wells and test set consisting of test wells to train and validate the proposed method, respectively. Cross validation is performed to determine the optimal combination of well logs and hyperparameters for permeability prediction. Core permeability is log transformed and all well logs, are min/max normalized to a minimum of -1 and a maximum of 1 to improve the performance of the gradient-based optimization method for machine-learning model training.
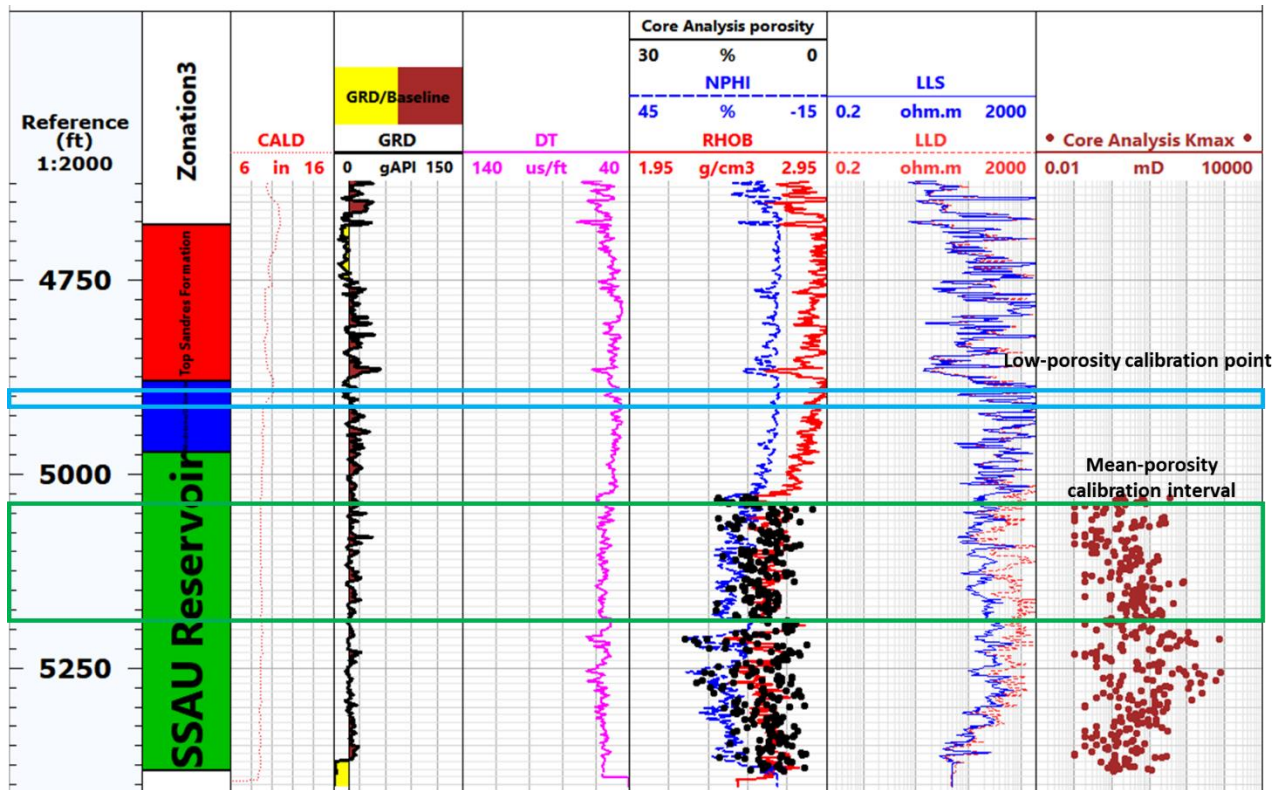
**Figure 3**. Input well logs and core data for quality control and workflow validation. There are three zones in this interval (Zonation, track 2), and we are interested in estimating the permeability (Core Analysis Kmax) of the "SSAU Reservoir" production zone using the caliper log (CALD), gamma ray log (GRD), sonic log (DT), neutron (NPHI) and density (RHOB) porosity logs and resistivity logs (laterolog LLD, LLS). Conventionally, well logs are normalized with the two-point scaling method to reproduce the univariate statistics of well logs from the type wells. One end point is chosen from the anhydrite/dolomite interval (blue) overlaying the production zone (green) while the remaining end point is selected from the dolomite facies in the production zone (green).

## DA Model Structure

The proposed DA model has a model structure similar to that of the generative adversarial neural networks (GAN). As shown in Figure 4, there are two neural networks in the DA model, the first one is denoted as the *generator* ($G$), while the second one is denoted as the *discriminator* ($D$). During training, the discriminator is optimized to distinguish the normalized well logs and petrophysical estimates of the type wells from those of the test wells, and output 1 for the type wells and 0 for test wells. The generator is optimized to calculate the normalized well logs and predict formation properties in the test wells, such that the statistical distributions of well logs and properties are similar to those of the type wells, making the discriminator fail to distinguish the outputs of the generator from the data of the training set

(update 2 in Figure 4). The generator is also responsible for minimizing the prediction errors in type wells (update 1 in Figure 4). Both generator and discriminator are trained adversarially until the generator outputs normalized well logs and formation property estimates for the test wells that reproduce the statistics observed for type wells, and Nash's equilibrium is reached (Goodfellow et al., 2014). Due to noise and bias present in well logs, which are caused by various borehole environmental conditions, e.g., irregular caliper, noisy and inadequate measurements, wells penetrating similar formation properties may exhibit different well logs.

The generator can be further divided into two parts (Figure 4), the preprocessing layers ($P$) normalizing well logs and the mapping layers ($M$) mapping normalized well logs to formation properties. Preprocessing layers calculate normalized well logs ($\tilde{X}_s, \tilde{X}_t$) from well logs of the training set ($X_s$) and test set ($X_t$) with the same structure but different weights and biases ($P_s, P_t$); when $P_s$ is an identical mapping, and $P_t$ is a linear mapping, the preprocessor is equivalent to the conventional linear normalization. Mapping layers ($M$) for $\tilde{X}_s$ and $\tilde{X}_t$ are the same, where formation property estimates for the training set ($\tilde{Y}_s$) and the test set ($\tilde{Y}_t$) are calculated. Mapping layers are optimized to minimize the prediction errors of the training set ($X_s, Y_s$), cross validation is applied to obtain optimal weights and biases of mapping layers that avoid overfitting. Mapping layers are the only layers that exist in a conventional, unconstrained machine-learning model. In the DA model, mapping layers can be a pre-trained machine-learning model or a classical petrophysical model that do not overfit the training data. Algorithm 1 below summarizes the training process of the asynchronized discriminative adversarial model.

| |
|---|
| **Algorithm 1**: Asynchronized discriminative adversarial model for petrophysical interpretation. |
| 1. Calibrate petrophysical models or train machine-learning models ($P_s, M$) according to Eq. 3, with the training data ($X_s$ and $Y_s$) from type wells and perform K-fold cross validation to avoid overfitting of the training data.<br>2. Fix and save the model parameters obtained in the first step.<br>3. Use the model obtained in the previous step to calculate $\tilde{Y}_s$ and $\tilde{Y}_t$ with $X_s$ and $X_t$, respectively.<br>    **For** number of training iterations do<br>      • Sample minibatch $x_s, \tilde{y}_s$ from $X_s, \tilde{Y}_s$, and $x_t, \tilde{y}_t$ from $X_s, \tilde{Y}_t$<br>      • Update the discriminator ($D$) by descending the discriminator loss of Eq. 1<br>      • Update the preprocessing layers for the test set ($P_s$) by descending the generator loss of Eq 2*<br>    **End for**<br>4. Save the weights of $P_s$ when the $\mathcal{L}_{adv_{GC}}$ is small.<br>5. Make prediction for the test set with $P_s$ and $M$. |

The objective functions for the discriminator and the generator are given by

$$\min_{D} \mathcal{L}_{adv_D}(X_s, X_t, P_s, P_t, M) = -\mathbb{E}_{x_s}\left[\log D\left(M\big(P_s(X_s)\big)\right)\right]$$
$$- \mathbb{E}_{x_t}\left[\log\left(1 - D\left(M\big(P_t(X_t)\big)\right)\right)\right] \tag{1}$$

$$\min_{P_t} \mathcal{L}_{adv_G}(X_t, M, D) = -\mathbb{E}_{x_t}\left[\log D\left(M\big(P_t(X_t)\big)\right)\right] \tag{2}$$

$$\min_{P_s, M} \mathcal{L}_{pred}(X_s, Y_s) = \mathbb{E}_{x_s, y_s}\left[\left\|Y_s - M\big(P_s(X_s)\big)\right\|_2\right], \tag{3}$$

where $\mathcal{L}_{adv_D}$ is the discriminator adversarial loss and $\mathcal{L}_{adv_G}$ is the generator adversarial loss. The $\mathcal{L}_{pred}$ term in Eq. 3 is the mean-squared error (MSE) of the prediction for the continuous response feature and can be replaced with categorical cross entropy for categorical output or other types of errors that are commonly used in machine-learning models. The mapping layers can be replaced with pre-trained petrophysical or machine-learning models, and in these cases, Eq. 3 is not used to train the pre-trained models to avoid overfitting. The model trained with Eq. 3 only is denoted as the original (unconstrained) model because no preprocessing layers are used for well-log normalization.

When bias between the well logs of the training and test sets is deemed negligible, high certainty should be assigned to unconstrained predictions and slight normalization should be performed to avoid over alignment. In this latter case, an additional loss term to quantify the certainty of unconstrained prediction is imposed to Eq. 2, such that Eq. 2 is modified into Eq. 2* as follows:

$$\min_{P_t} \mathcal{L}_{adv_{GC}}(X_t, P_s, M, D, \lambda) = -\mathbb{E}_{x_t}\left[\log D\left(M\big(P_t(X_t)\big)\right)\right] \tag{2*}$$
$$+ \lambda\mathbb{E}_{x_t}\left[\left\|M\big(P_t(X_t)\big) - M\big(P_s(X_t)\big)\right\|_2\right],$$

where $\lambda$ quantifies the certainty of unbiased well logs in the test set and $\lambda$ is set to 0 in our workflow to impose high uncertainty to test well logs. The $L_2$ constraint term ($\| \quad \|_2$) can be replaced with other types of loss functions for the prediction of other types of formation properties, such as categorical cross entropy for categorical output for rock facies prediction; $M\big(P_t(X_t)\big)$ is equal to $\tilde{Y}_t$ in Algorithm 1.
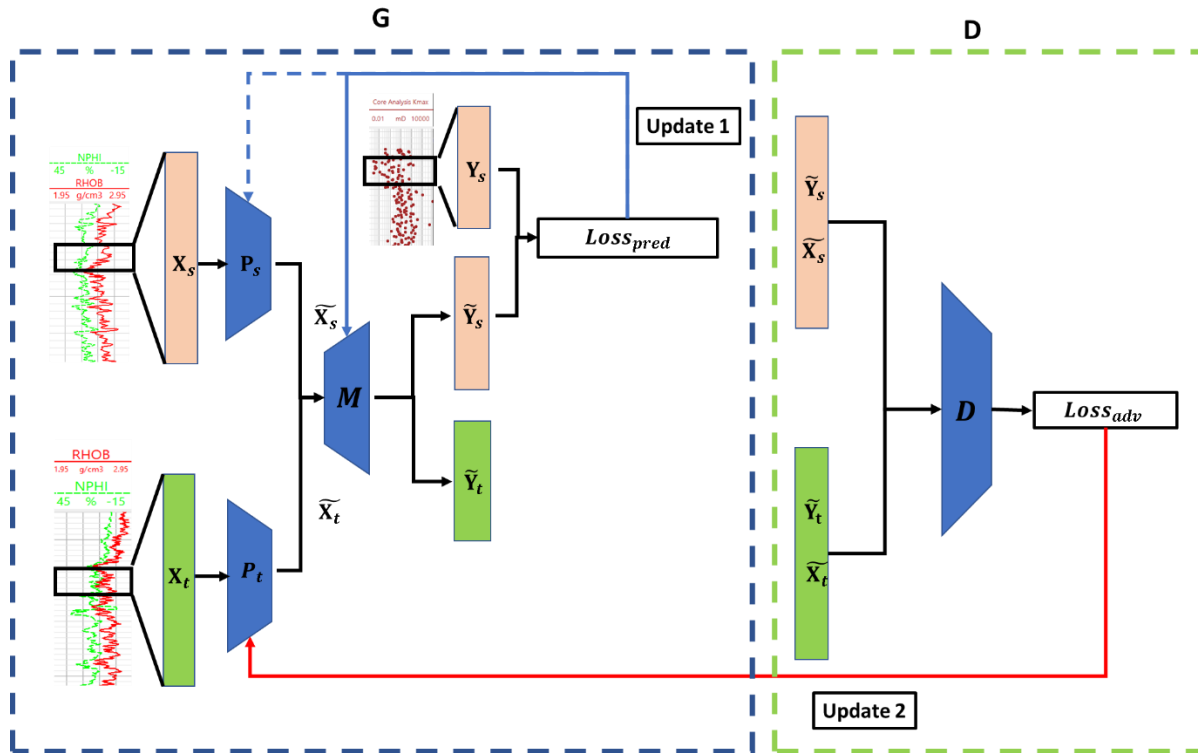
**Figure 4**. Structure of the Discriminative Adversarial (DA) model. Two loss functions are optimized asynchronously (red, blue lines), $P_s$ is updated (dashed line) when it is not an identical mapping and normalized logs of the test set are not output.

When a pre-trained model is used as the mapping layers, and the gradient is not accessible, such as tree models and black-box commercial interpretation algorithms, a simple model, such as the random forest (RF) is used as the discriminator. The RF discriminator calculates the $\mathcal{L}_{adv_D}$ with cross validation to avoid overfitting, and the optimum model parameters for $P_s$ are obtained through grid search.

## Model with Linear Constraints

The DA model normalizes well logs by imposing the DA loss constraints; it is important to compare the DA constraint to other common constraints. Therefore, we compare the DA model to the machine-learning model with linear model constraints. The linear constraint model has the same model structure as the DA model, except that it does not use the DA loss to optimize the preprocessing layers; instead, it optimizes the preprocessing so that the output permeability estimates are consistent with the predictions obtained from the unconstrained model and all types of linear models.

The linear models used include a linear spatial stationarity model for permeability, and linear models between well logs with high certainty and permeability. With the spatial stationarity

constraint and linear models between well logs and permeability, we can decrease the model variance and improve the prediction accuracy with well logs with high certainty and by assuming spatial stationarity of the permeability distribution. The assumption made for the linear constraint model is that the distribution of formation property, i.e., logarithmic permeability, is stationary and that the distribution of the prediction error of the linearly constrained model is also stationary.

To impose the stationarity constraint for a test well and associated type well(s), the mean value of a formation property, the global proportion of different facies, and their spatial covariance are assumed (regionally) stationary and used to perform the prediction of formation properties. Due to the spatial heterogeneity of the reservoir, properties such as permeability have limited spatial continuity; therefore, for permeability prediction, we only use the mean value to constrain the estimation, i.e.,

$$\overline{Y}_s = \mathbb{E}_{y_s}[Y_s], \tag{4}$$

where $\overline{Y}_s$ is the average value of the formation property of type wells for a test well. For continuous formation property estimation, such as porosity and facies prediction, the kriging method is used to perform the prediction.

To impose the linear well-log interpretation model constraint, a simple linear model or petrophysical model are used to predict formation properties from well logs that are believed less likely to be affected by the borehole logging environment and logging tools, e.g., density log (RHOB), i.e.,

$$\min_{A,B} \mathcal{L}_{linear}(X_{s_u}) = \mathbb{E}_{x_s,y_s}\left[\left\|AX_{s_u} + B - Y_s\right\|_2\right] \tag{5}$$
$$\tilde{Y}_{s_l} = AX_{s_u} + B,$$

where $A$ and $B$ are coefficients of the linear model calibrated with the training data, $X_{s_u}$ are the reliable well logs of type wells for a test well, and $\tilde{Y}_{s_l}$ is the prediction of the linear model for the training set.

To combine different types of linear predictions, the covariance matrix of the predictions of different models is used to weight the predictions from different models. The variance of the ML model predictions is calculated with the K-fold cross validation, i.e., the covariance between predicted and true formation properties of the validation set instead of training set are calculated and used to represent uncertainty of different predictions, thereby constraining the prediction of the complex mapping model and avoiding potential overfitting; the corresponding loss function is written as

$$C_d = \begin{bmatrix} \dfrac{Cov(M(P_s(X_s)),Y_s)}{\lambda_l^2} & \dfrac{Cov(M(P_s(X_s)),\overline{Y}_s)}{\lambda_l} & \dfrac{Cov\left(\tilde{Y}_{s_l},M(P_s(X_s))\right)}{\lambda_l} \\[2em] \dfrac{Cov(M(P_s(X_s)),\overline{Y}_s)}{\lambda_l} & Cov(\overline{Y}_s,Y_s) & Cov(\overline{Y}_s,\tilde{Y}_{s_l}) \\[2em] \dfrac{Cov\left(\tilde{Y}_{s_l},M(P_s(X_s))\right)}{\lambda_l} & Cov(\overline{Y}_s,\tilde{Y}_{s_l}) & Cov(\tilde{Y}_{s_l},Y_s) \end{bmatrix} \tag{6}$$

$$E = \left[M\big(P_t(X_t)\big) - M\big(P_s(X_t)\big); \; M\big(P_t(X_t)\big) - \overline{Y}_s; \; M\big(P_t(X_t)\big) - \big(AX_{t_u} + B\big)\right]$$

$$\min_{P_t} \mathcal{L}_{lc}(X_s, X_t, Y_s, P_s, M) = \mathbb{E}_{x_t}[E^T C_d^{-1} E],$$

where $Cov$ is the covariance of the predictions of two methods, $\lambda_l$ is similar to $\lambda$, quantifying the certainty that well logs of a test well and associated type wells have the same logging environment, $E$ is the array of differences between different predictions, and $\mathcal{L}_{lc}$ is the linear constraint imposed to Eq. 3. During training, the linear constraint (Eq. 6) instead of the adversarial loss (Eqs. 1,2) is optimized after the optimization of the $P_s$ and $M$ in Eq. 3.

## Identification of Type Wells

For both distance-based and divergence-based type well identification methods, type well(s) for a test well should be selected based on the similarity of their formation properties. Based on the stationarity of formation properties at different well locations, either a stationary well or a type well method should be used. If the formation property is stationary among wells, all type wells are used to build the training set, whereas if only regional stationarity exists, well(s) statistically or spatially closest to a test well should be used to build the training set for the test well.

Cross plots and histograms of well logs and core measurements of all the wells are visualized and analyzed to support the stationarity assumption for the reservoir and find potentially biased test wells. Additionally, to ascertain the statistical similarity between type wells and test wells, the KL divergence of well-log joint distribution of each pair of wells is calculated with the nearest-neighbor method (Wang, et al., 2009) and visualized with multi-dimensional scaling (MDS) (Borg and Groenen, 2005).

Type wells should be selected to have formation properties similar to those of a test well. To quantify the similarity between a type well and a test well, there are two types of distances that can be used: the first one is based on the spatial distance, i.e., a type well for a test well is the well spatially closest to the test well. This type of well identification method is consistent with the conventional type well method (Shier, 2004), and assumes spatial continuity, where two

adjacent wells should exhibit similar formation properties. Another distance is the statistical distance of well logs, i.e., the KL divergence between the well logs of each pair of wells are calculated (Pérez-Cruz, 2008; Sasaki et al., 2015), and the well with the smallest divergence to the test well is identified as the type well, which does not rely on the assumption of spatial continuity. When formation properties are non-stationary, zone thickness varies much at different well locations, wells penetrate different zones, and well spacing is large; hence the divergence-based type well should be used, e.g., in a deepwater turbidite system the divergence between well-log joint distributions of wells penetrating channel sandstones and wells penetrating the overbank shale is large, while spatially close wells do not necessarily penetrate the same architectural elements or stratigraphic intervals, especially when well spacing is large. Therefore, in this study, three training and testing splitting strategies are discussed: 1) the *spatial distance-based type well method,* which assumes a non-stationary formation property distribution and identifies type wells for each test well with spatial distance, 2) the *statistical distance-based type well method,* which assumes non-stationary formation property distributions and identifies type wells for each test well with divergence, and 3) the *stationary well method,* which assumes a stationary formation property distribution and identifies type wells for all test wells with divergence. For methods (1) and (2), the weights of mapping layers vary for different test wells, while for method (3), only one set of mapping layers is trained with all the data from all training wells.

## Design of Numerical Experiments

Our proposed interpretation workflow is compared to the conventional machine-learning workflow without constraint, with two-point scaling and with linear constraints, where the two-point scaling method uses the 10% and 90% quantiles to perform the normalization. The $P_s$ and $M$ layers are identical for all three workflows, and only the normalization layers of the test set, $P_t$, vary in different workflows. In conventional machine-learning workflows, $P_t = P_s$ in the DA workflow, $P_t$ is determined through Eq. 2*, while in the model with linear constraints, $P_t$ is determined through Eq. 6. Three different training well selection methods discussed in the previous section are compared, and the training testing data split is based on the jackknife test method, a.k.a. the leave-one-out validation method, i.e., each time a well is selected from all wells as the test well while the type wells are selected from the remaining wells. For both type well methods, one training well is selected for each test well, while for the stationary well method, 6 training wells that are most representative are selected for all test wells. A total of 12 conditions are discussed. We apply these methods to solve the permeability estimation problem, where the permeability estimates are validated against core measurements. The performance of different conditions is evaluated based on the MSE of permeability predictions.

# Results

## Well-Log Visualization

We visualize the pairwise cross plots (bivariate joints) and the marginal distribution of well logs from all wells in Figure 5. Cross plots between porosity core measurements (CPOR) and permeability core measurements (CKMAX) from different wells are similar, indicating a stationary carbonate reservoir. Cross plots and histograms of well logs indicate that biases exist in the sonic logs (DT) and neutron logs (NPHI) of some of the wells, which will be corrected with our normalization models in the following sections.
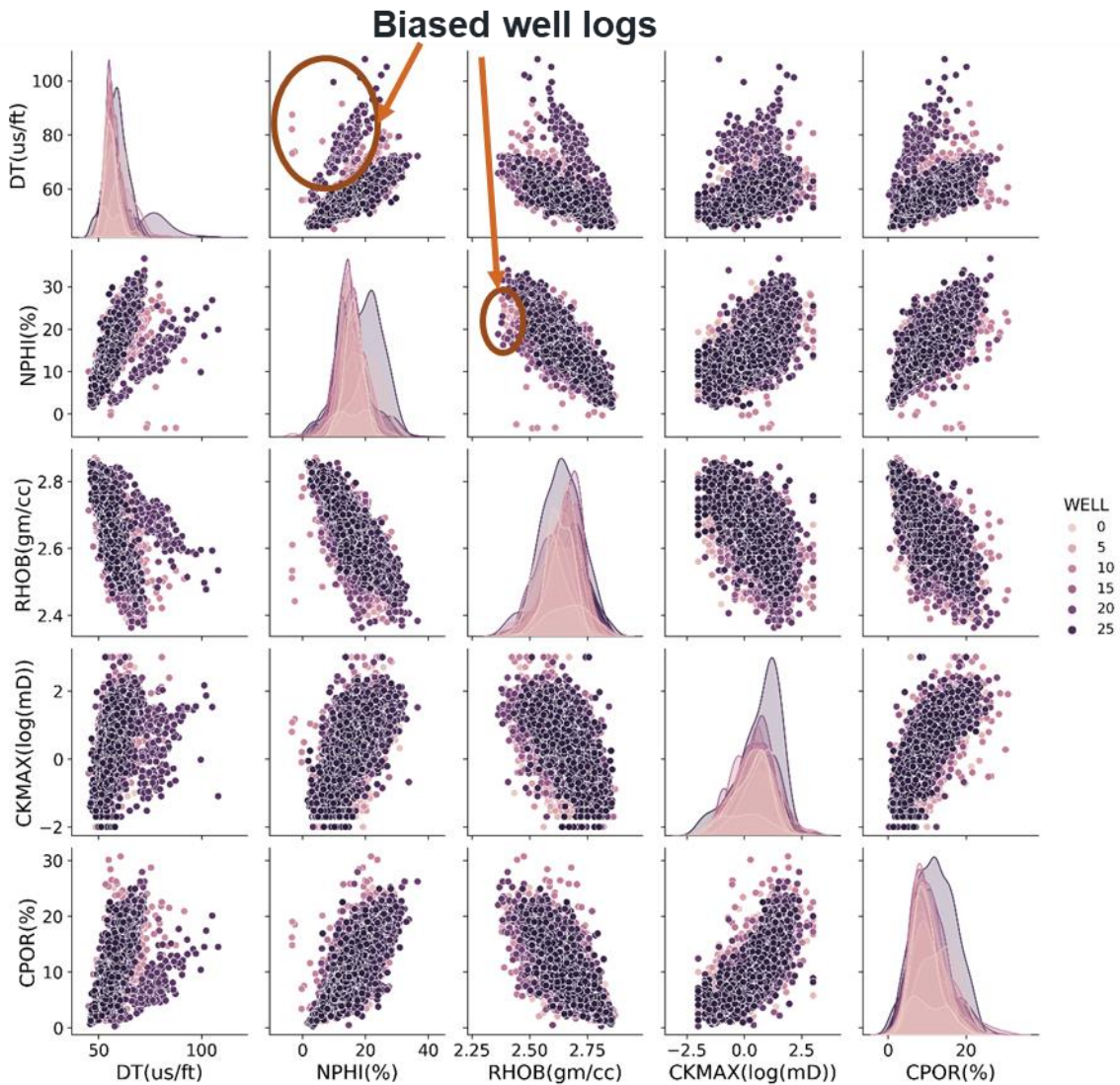
**Figure 5**. Histograms and pair-wise scatter plots of sonic (DT), neutron (NPHI), density (RHOB), core permeability (CKMAX) and core porosity (CPOR) logs of all wells. From the scatter plots we observe that some wells have biased sonic logs, resulting in a different trend between the sonic log and other types of well logs.

Even though formation properties from core measurements are stationary, the bias introduced by the measurement environments, such as different logging tools, vendors, and vintages may not be stationary; therefore, we also compare results obtained with both the *stationary well method* and the *type well method*.

## Training and Test Well Splitting

Figure 6 shows the locations of all the wells available for our study. For the distance-based type well identification method we select training wells as the wells closest to the test wells. To better capture the statistical similarity of well logs between wells, the KL divergence between each pair of wells is calculated and summarized as the distance matrix in Figure 7; it is obvious from the distance matrix that well 9 and well 24 have well-log joint distributions that are different from those of other wells. Therefore, we refer to them as the outlier test wells. In Figure 8, the 2D multiple dimensional scaling (MDS) map calculated from the KL divergence matrix helps to visualize the statistical distance between the wells. In the stationary well method, wells with the smallest distances to the center of the well cloud are denoted as the training wells (green), while in the divergence-based type well method, the well statistically closest to a test well is identified as the training well.
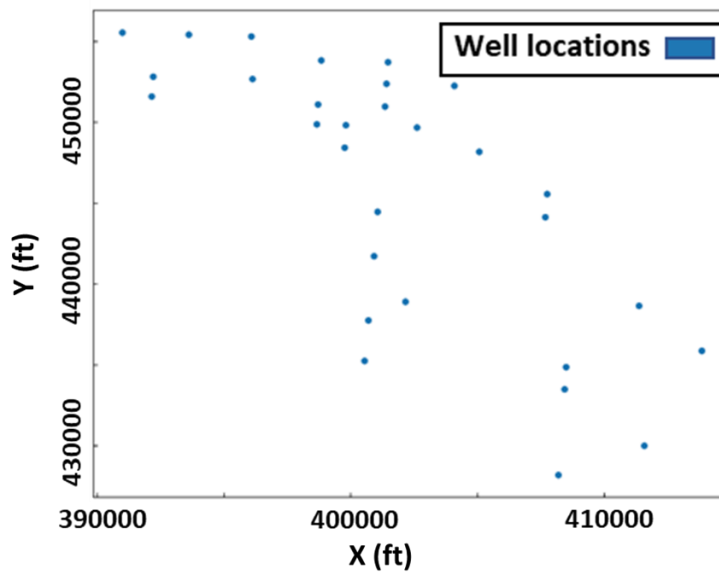
**Figure 6**. Well head locations of wells at SSAU. Core measurements are available for these wells to calibrate and validate different models.

# Petrophysical Interpretation via Machine-Learning and Statistical Models

**Figure 7**. Statistical Distance Matrix representing the statistical distance between any pair of existing wells. The statistical distance between a pair of wells is calculated as the K-L divergence of the well-log joint distribution between the wells.
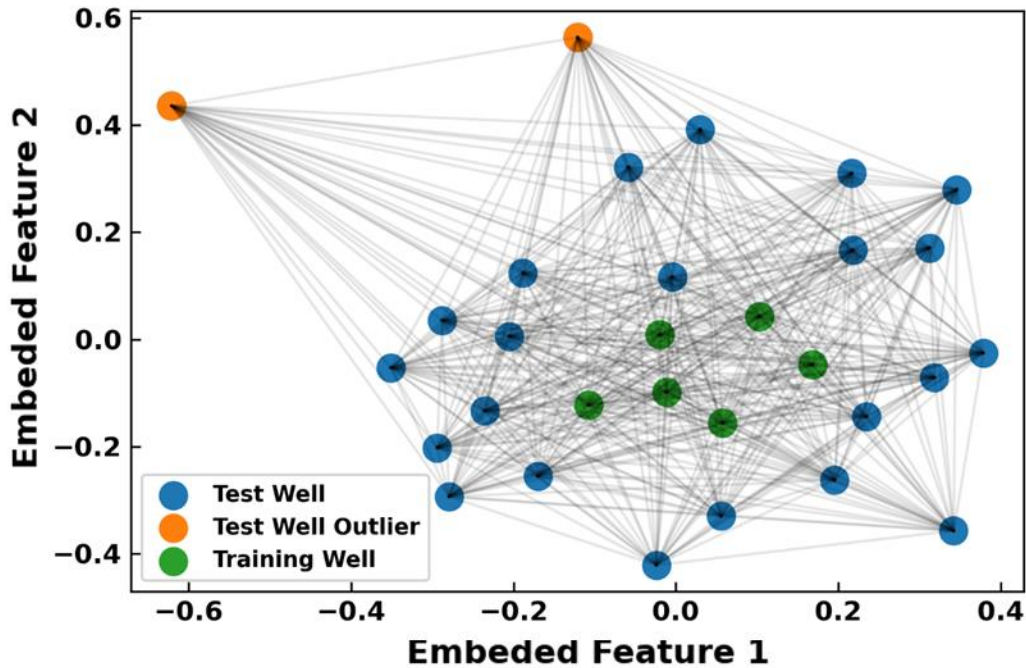


**Figure 8**. MDS map calculated based on the statistical distance of the available wells. Test wells (blue) and training wells (green) are statistically similar, while outlier test wells (orange) are statistically different from other wells; lengths of lines between wells represent their pair-wise statistical distances on the two-dimensional MDS feature space.

## Permeability Estimation

Permeability estimation for all test wells is performed with the 12 combinations of methods and the corresponding results are compared among them. Tables 2 and 3 summarize the MSE of the permeability predictions. The following observations stem from the two tables:

(1) Compared to models without constraints, all types of constraints discussed above improve the performance of the permeability prediction model.
(2) For outlier test wells, the DA model combined with the stationary type well identification method yields the best permeability estimates.
(3) For non-outlier test wells, the DA model combined with the divergence-based type well identification method yields the best permeability estimates.

(4) For training well selection strategy, the distance-based type well method exhibits the highest MSE, regardless of the constrained model used. The differences between permeability predictions obtained the divergence-based type well and stationary well methods are small for test wells that are not outliers.

| | No constraint | Two-point scaling | Linear constraint | DA loss constraint |
|---|---|---|---|---|
| **Divergence-based type well** | 0.76077 | 0.800165 | 0.617754 | 0.628871 |
| **Distance-based type well** | 1.25534 | 0.740518 | 0.652266 | 0.91469 |
| **Stationary well method** | 1.6299 | 0.653783 | 0.691621 | 0.588523 |

**Table 2**. MSE of logarithmic permeability estimation for outlier test wells. Without proper constraints, the MSE can be greater than one order of magnitude (1.6299). Adding constraints and properly scaling the well logs helps to decrease the error.

| | No constraint | Two-point scaling | Linear constraint | DA loss constraint |
|---|---|---|---|---|
| **Divergence-based type well** | 0.584184 | 0.529513 | 0.452425 | 0.427909 |
| **Distance-based type well** | 0.745191 | 0.592629 | 0.517844 | 0.595696 |
| **Stationary well method** | 0.571057 | 0.509348 | 0.453453 | 0.438051 |

**Table 3**. MSE of logarithmic permeability estimation for non-outlier test wells. Adding constraints and properly scaling the well logs helps to increase the accuracy of the permeability prediction.

Permeability estimates and permeability core measurements from the outlier well 24 are compared in the first four tracks in Figure 9. Compared to the estimate without normalization (K_origin), the two-point scaling, DA constraint, and linear constraint methods yield the best permeability estimates.  Permeability prediction with the DA method (K_DA) has the lowest MSE. For tracks 5 to 8, the normalized and original well logs are compared, the correction to sonic log (DT) is large for all three methods, and the DA constraint method predicts the lowest normalized compressional slowness compared to other methods.  While differences between normalized and original nuclear logs are small for the DA method, well logs normalized with the linear constraint method are smoother than the original well logs, and the average value of the density log normalized with the two-point scaling method decreases 3% compared to the original density log.

Figure 10 summarizes the multivariate statistics of normalized well logs and permeability. Compared to other methods, the variance of permeability predicted with the linear constraint

method (K_linear) decreases 23% on average, while the correlation coefficient of normalized well logs increases 11 % on average. Marginal distributions of normalized well logs calculated with both the two-point scaling and DA methods match those of the training wells.
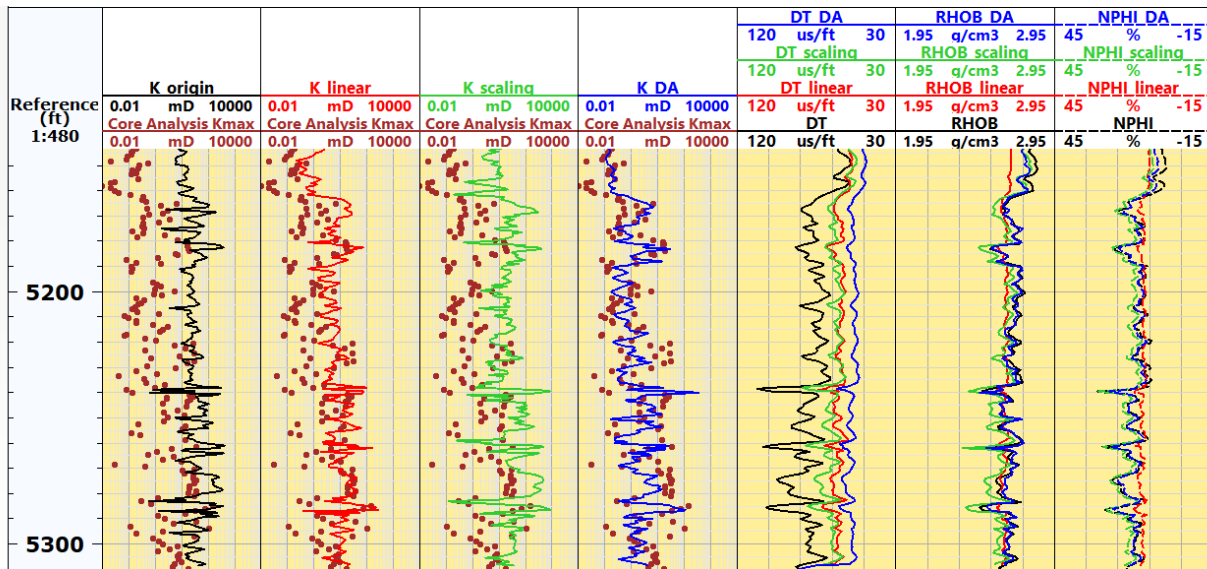


**Figure 9**. Permeability estimates for the outlier well No. 24 based on 6 stationary training wells. Comparison of results obtained for the unconstrained model (black with suffix "_origin"), linearly constrained model (red with suffix "_linear"), two-point scaling normalized model (green with suffix "scaling"), and DA model (blue with suffix "_DA"). The first four tracks show the actual and predicted permeability, while the next three tracks show the original and normalized sonic (DT), density (RHOB) and neutron (NPHI) well logs.
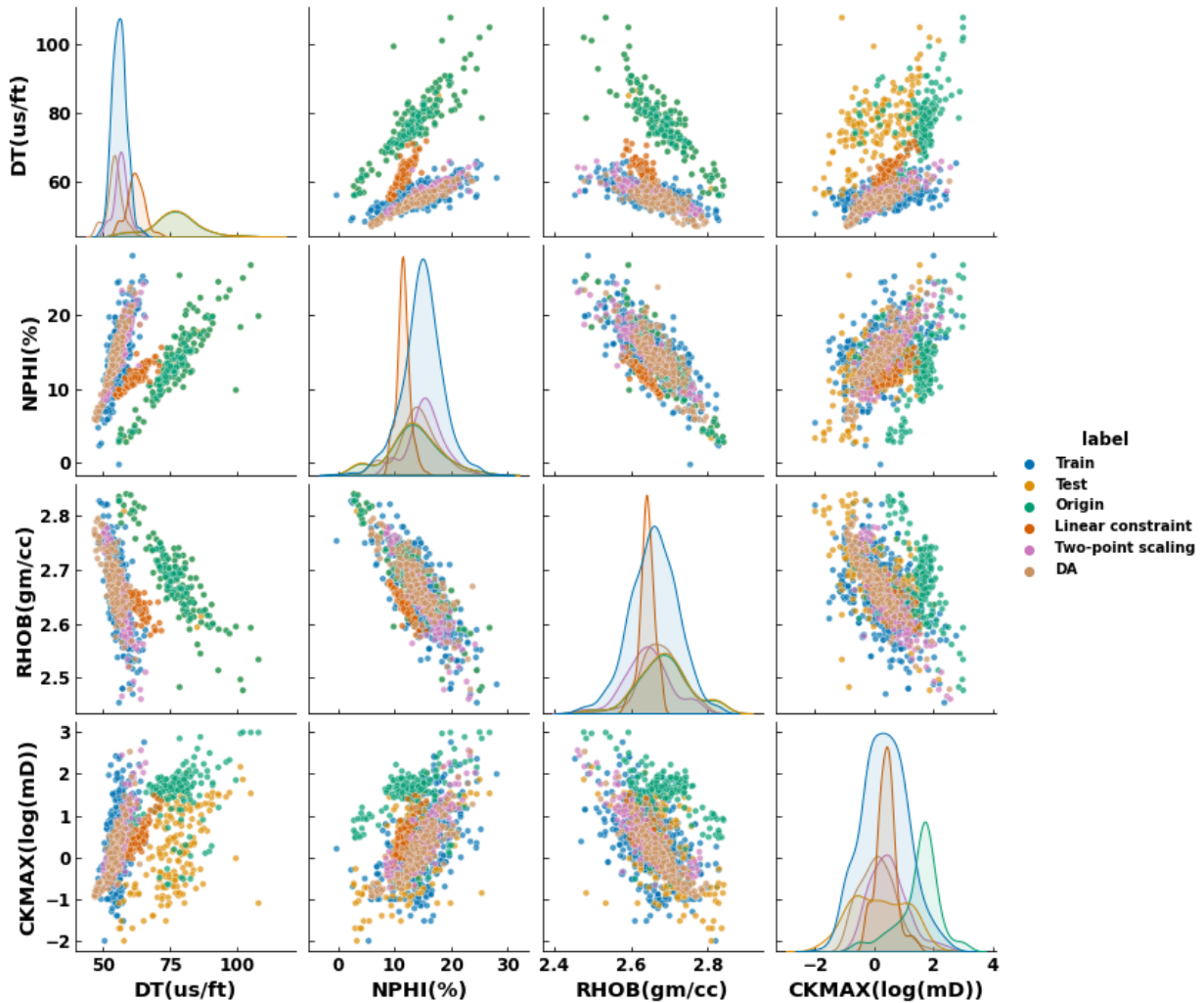
**Figure 10**. Cross-plots and histograms of normalized well logs and permeability of an outlier test well. The distribution of well logs (orange, "Test") of the outlier test well is different from that of the training well logs (blue. "train"). Predictions obtained without well-log normalization (green, "Origin") overestimate the permeability due to the biased sonic log; the prediction and normalized well logs calculated with the linear constraint method (red, "Linear constraint") have a smaller variance and a higher correlation than those calculated with other methods. Normalized well logs calculated with the two-point scaling method (pink, "Two-point scaling") reproduce the univariate statistics of the training well logs, while normalized well logs calculated with the DA method (brown, "DA") and reproduce the joint distribution of the training well logs.

Figure 11 compares the permeability estimates and normalized well logs from one of the non-outlier test wells. Estimation errors are low for all four methods, and corrections to well logs are small for the DA and two-point scaling methods, while the linear constraint method

smooths and increases the sonic log after normalization. The pairwise, multivariate statistics of well logs and permeability estimates in Figure 12 show that the normalized logs are similar to the training well logs except for the linear constraint method.
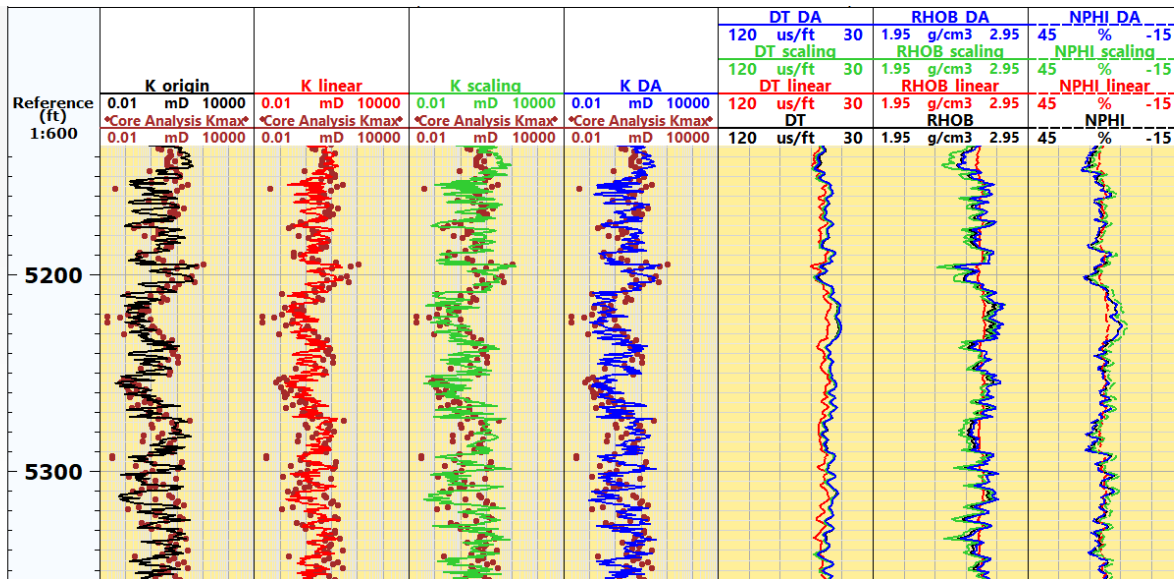


**Figure 11**. Normalized well logs of a non-outlier test well. Comparison of permeability predictions obtained with the unconstrained model (black with suffix "_origin"), linearly constrained model (red with suffix "_linear"), two-point scaling normalized model (green with suffix "scaling"), and DA model (blue with suffix "_DAs"). The first four tracks show the actual and predicted permeability, while the next three tracks show the original and normalized sonic (DT), density (RHOB) and neutron (NPHI) logs.

Petrophysical Interpretation via Machine-Learning and Statistical Models
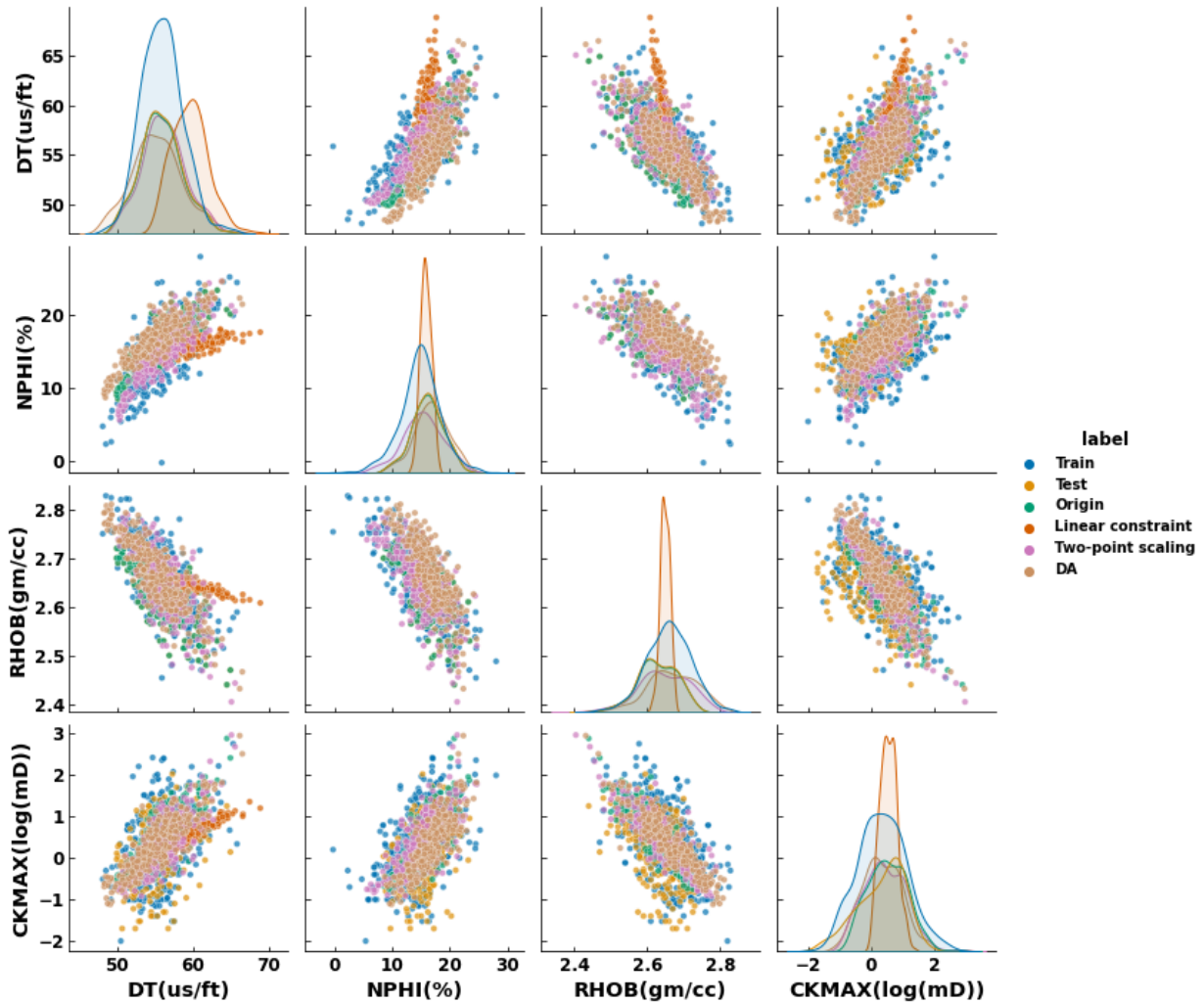
**Figure 12**. Cross-plots and histograms of normalized well logs and permeability obtained from a non-outlier test well. The distribution of well logs (orange, "Test") from this well exhibits univariate and pairwise statistics similar to those of the training well logs (blue. "train"). Permeability predictions and normalized well logs calculated with the original (green, "Origin"), DA (brown, "DA"), and two-point scaling (pink, "Two-point scaling") methods all reproduce the distribution of the training well logs, while permeability estimates and normalized well logs calculated with the linear constraint method (red, "Linear constraint") have smaller variance and higher correlation compared to other methods.

The KL divergence of well logs and permeability estimates between the test and type wells is calculated for every iteration of DA (blue) model training, and the final iterations of two-point scaling (red) and unconstrained (yellow) models. Figure 13 compares the KL divergence with the MSE of permeability prediction. In Figure 14, the discriminator accuracy is calculated and compared to the MSE of permeability prediction.

A strong correlation exists between the KL divergence and the MSE of permeability prediction and between the discriminator accuracy and the MSE. Because the DA model training is an iterative optimization process, we determine the optimal permeability estimates of the DA model by only keeping the iteration with the lowest KL divergence/ discriminator accuracy. Although the two-point scaling method sometimes has a lower KL divergence, the DA method yields more accurate permeability estimates. Compared to the other two methods, the DA method has the lowest discriminator accuracy.



(A)        (B)
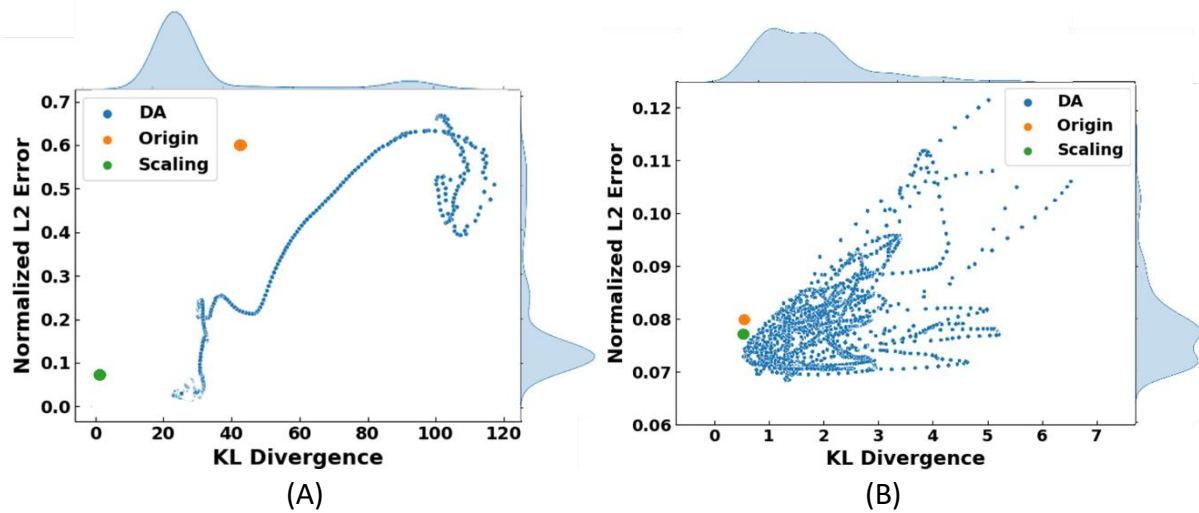
**Figure 13**. The KL divergence vs. the MSE of permeability prediction from 3 constrained models at different training epochs for an outlier test well (A) and a normalized well (B). A lower divergence indicates that the normalized well logs better reproduce the distribution of training well logs. Training of all three constrained models decreases the divergence and better estimates the permeability. The DA model at its lowest divergence point (blue) has the lowest error, followed by two-point scaling method (red) and the original model (yellow). Also, the two-point scaling method may have lower KL divergence than the DA model (A) due to over alignment. The DA model training is an iterative optimization process: the error does not monotonically decrease or increase; instead, the model normalizes well logs and makes predictions to explore the solution space iteratively, guided by discriminators optimized at different epochs, where the optimal output can be determined as the point with the lowest KL divergence.

(A)                                                                    (B)
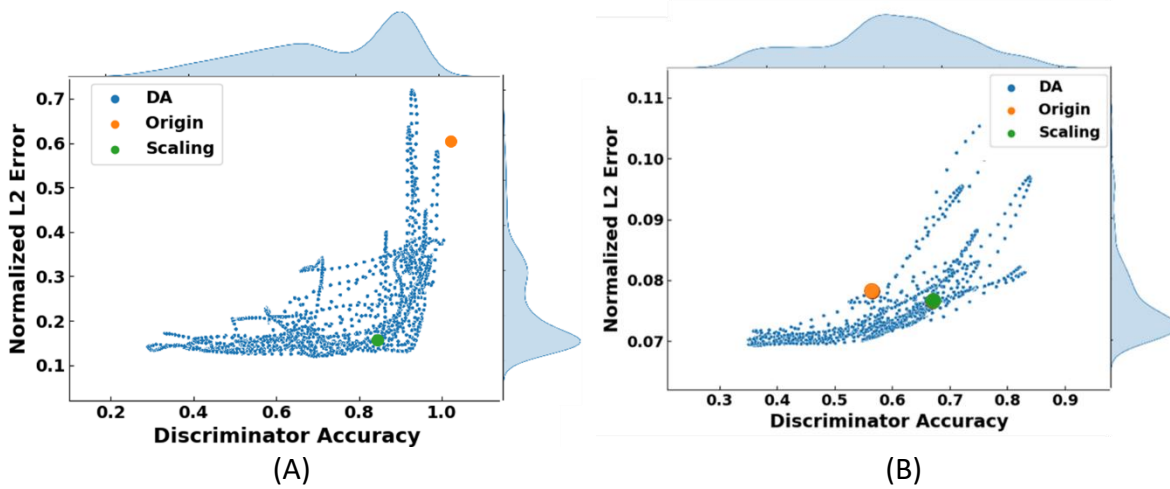
**Figure 14**. Accuracy of the discriminator vs. the MSE of permeability estimates at different training epochs of three constrained models for an outlier test well (A) and a non-outlier test well (B). Permeability calculated with the DA method (blue) has the lowest prediction error, followed by the two-point scaling method (red) and the original model (yellow). The DA method has the lowest discriminator accuracy. The DA model training is an iterative process, where the discriminator accuracy oscillates between 0 and 1 during the training, and the optimal output can be determined as the training epoch with the lowest discriminator accuracy at a late training stage.

In Figure 15, cross-plots of predicted permeability and permeability core measurements indicate that no obvious bias exists in any of the predictions obtained with the four methods, while the DA method has the lowest error.
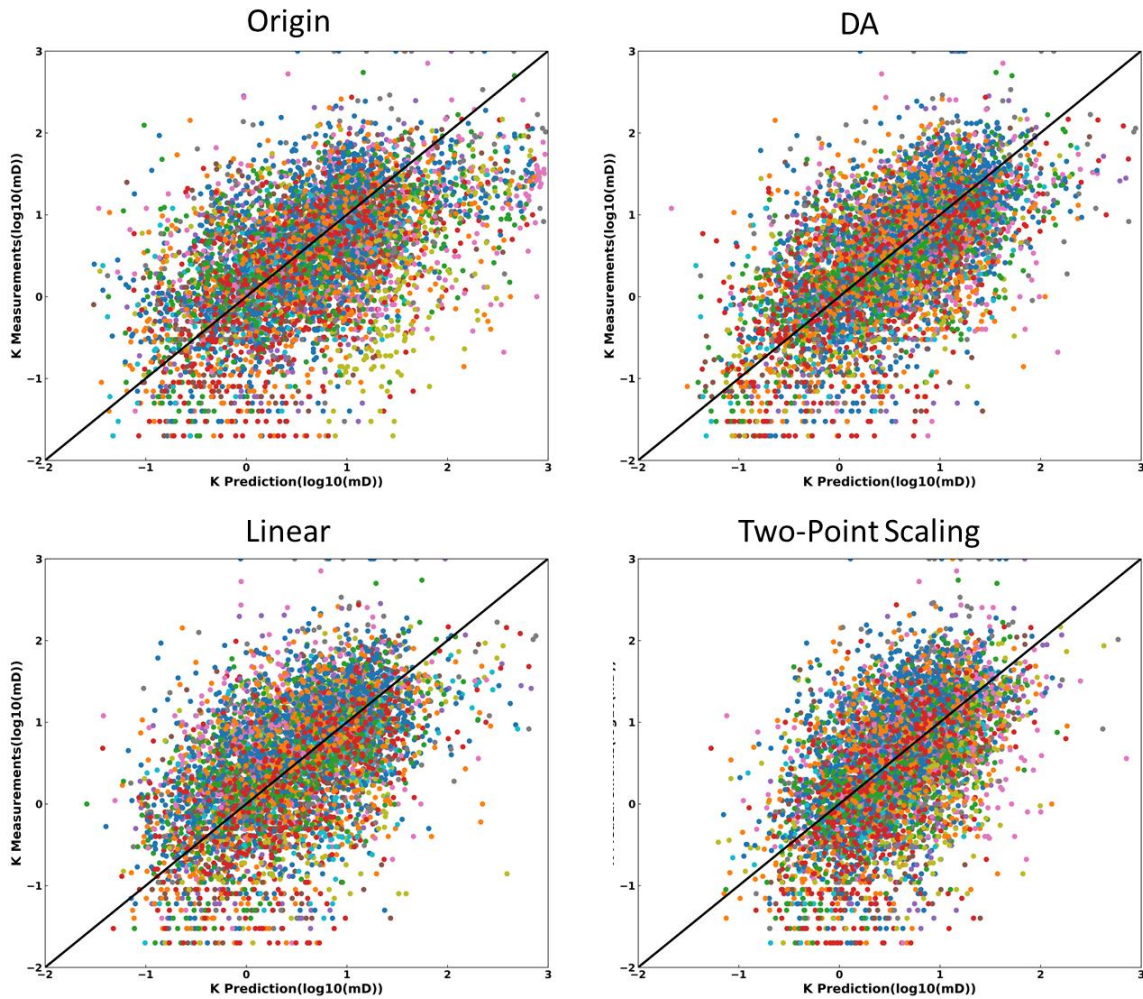
**Figure 15**. Cross-plots of actual permeability and permeability estimates, with no obvious bias found for different methods. Log-transformed permeability core measurements (y axis) are compared to log-transformed permeability estimates from different models (x axis); data with the same color are from the same well, no obvious per well bias observed. Low-permeability rocks are not well identified due to both low quality of core measurement and complexity of the pore network for dolomite; the cloud does not deviate from the identical line, indicating an overall unbiased estimation.

# Discussion

## Type-Well Selection Strategy

As shown in Tables 2 and 3, permeability estimates calculated with the distance-based type well method have the highest error compared to the divergence-based methods, indicating a non-stationary formation property distribution and/or different environmental effects between spatially adjacent wells. Wells that are spatially close to each other do not necessarily have similar formation property distributions or borehole environments, resulting in different statistics of well logs in adjacent wells, which introduces the non-uniqueness and measurement bias and degrades the performance of machine-learning models. Divergence-based type well and stationary well methods mitigate this adverse behavior by training machine-learning models with only the training wells with small well-log joint distribution divergence to test wells, i.e., the distribution of well logs and formation properties of the test wells are similar to those of the training wells, and the training data are better adapted to the test data.

For outlier test wells, the stationary well method has better performance than the divergence-based type well method. Outlier test wells have formation property statistics or borehole environments that are very different from other wells, whereby it is difficult to find training wells with formation properties and borehole environments similar to those of the outlier test wells. Consequently, constraining the interpretation with global unbiased statistics yields better permeability estimations.

For other test wells, the divergence-based type well method is better than the stationary well method because wells with similar logging environments and formation property statistics are available, and only minor well-log normalization is needed for the prediction.

## Constraining Methods

According to Tables 2 and 3, the performance of different methods for imposing the stationarity constraint can be ranked as follows: top performance is for the DA method, followed by the linear constraint method, then the two-point scaling method, and the worst performance is for the original model without constraint.

Normalized well logs and permeability estimates obtained with the different methods vary in multivariate statistics as shown in Figures 9 and 12. The differences are as follows:

1. The linear constraint method constrains the original model with the average permeability and a simple linear relationship between reliable well logs and permeability. By decreasing model variability, the model is less prone to overfitting the training data, resulting in a stronger linear correlation between permeability estimates and well logs.

2. The two-point scaling method reproduces marginal distributions of well logs. It normalizes well logs to have small KL divergence to the training wells. However, failure to consider joint distribution of well logs and predicted permeability causes degradation of the estimation accuracy.

3. The DA method is designed to reproduce the joint distribution of well logs and permeability distribution (Fig. 4). However, it is found that the approximated KL divergence can be higher than for the two-point scaling method, as shown in Figure 13A. Two other possible explanations, besides an inaccurate KL divergence approximation, for this behavior are as follows: (1) the DA method is not likely to over align the training data, e.g., for a perfect discriminator and shallow $P_s$ layers, if the test set is a biased subset of the training set. The best strategy for $P_s$ layers to "fool" the discriminator is to perform an identical mapping instead of minimizing the KL divergence; therefore, the DA method is robust to potential over-alignment, (2) $P_s$ layers are trained to minimize the distance between the high-level features extracted by the discriminator instead of the divergence of the normalized well logs and permeability, i.e., discriminator accuracy (Figure 14); consequently, the associated features are better representations of the relationship between well logs and permeability.

4. The performance of the original model without any constraints is degraded by different borehole environmental conditions and the non-uniqueness of well-log interpretation.

Overall, the DA method yields the best permeability estimation by considering the multivariate statistics and high-level features extracted by the discriminator.

## Convergence of the DA Method

The training of the $P_s$ layers in the DA model is a dynamic process, i.e., the $P_s$ layers and the discriminator are optimized in an adversarial way. There is no clear indicator for the end of the training process for the DA model, i.e., the training continues as long as the training of the generator or discriminator do not overwhelm the training of the other. However, as shown in Figures 13 and 14, a strong correlation exists between the KL divergence, discriminator accuracy, and prediction mismatch. Therefore, we propose to use the discriminator accuracy or KL divergence to determine the end of training, where the training should be long enough to obtain a result with small discriminator accuracy and KL divergence, while the permeability estimates obtained at the iteration with the lowest possible discriminator accuracy or KL divergence are taken as the final prediction.

# Conclusions

For the first time, we provided geostatistical insights and assumptions of classical well-log normalization methods for consistent quantification of petrophysical properties from well logs acquired in multiple neighboring wells, i.e., the stationarity of formation properties. We found that statistical distance-based type well identification methods are better than the distance-based type well identification method for permeability prediction from well logs. While the permeability prediction error ((log mD)^2) of the distance-based type well identification method is between 0.51 and 0.91, the error of statistical distance-based type well identification methods is between 0.4 and 0.8. Compared to the distance-based method, the statistical distance-based method decreases the permeability prediction error by 20-40%. The statistical distance-based type well identification method improves the interpretation accuracy by better adapting test wells to training wells with borehole environmental conditions and formation properties similar to the test well. Therefore, we recommend using the divergence-based type well identification method for well-log normalization in test wells without obvious measurement biases and noise, and using the stationary type well identification method for test wells with well-log statistics very different from those of training wells.

With the two new, constrained, machine learning-based, multi-well petrophysical interpretation workflows introduced in this paper, i.e., the linearly constrained and DA models integrated with statistical distance-based type well identification strategy, we successfully decreased the petrophysical interpretation error introduced by logging vintage, vendors, and borehole environments of different wells, and greatly decreased the time and effort required for manual well-log normalization and interpretation. While the permeability prediction error without constraints is between 0.57 and 1.6, the error of permeability prediction with constraints is between 0.43 and 0.91. Compared to classical machine-learning models without constraints, the linear constraint model decreases the permeability estimation error by 10%-50%, while the DA model decreases the permeability estimation error by 20-60%. We found that the enforcement of proper constraints greatly improved the accuracy of petrophysical interpretation; hence, we propose to use either the DA model or the linear constraint model for machine-learning-based well-log interpretation.

Accurate formation properties predicted with our proposed statistical distance-based type well identification method and constrained machine-learning model help to construct reservoir models that provide more accurate reserve-volume estimates, production forecasts, and help with decision making in reservoir development.

Both the statistical distance-based type well identification method and the constrained machine-learning model assume that well logs are stationary among training and test wells, thus proper zonation is necessary for the successful application of our interpretation workflow. In the future, we will examine the possibility of performing automatic zonation to further automate the petrophysical interpretation procedure.

## List of Acronyms

| | |
|---|---|
| $CALD$ | Caliper log |
| $CKMAX$ | Maximum core permeability measurement (mD) |
| $CNN$ | Convolutional neural network |
| $CPOR$ | Core porosity measurement (v/v) |
| $DA$ | Discriminative Adversarial model |
| $DT$ | Sonic log (us/ft) |
| $GAN$ | Generative Adversarial Neural Network |
| $GRD$ | Gamma ray log (api) |
| $JS(D)$ | Jason-Shannon (divergence) |
| $K$ | Permeability estimates |
| $KL(D)$ | Kullback–Leibler (divergence) |
| $LLD$ | Lateral deep resistivity log |
| $LLS$ | Lateral shallow resistivity log |
| $MDS$ | Multi-Dimensional scaling |
| $ML$ | Machine Learning |
| $MMD$ | Maximum mean discrepancy |
| $MMDDT$ | Maximum mean discrepancy domain transfer (learning) |
| $MSE$ | Mean-squared error |
| $NPHI$ | Neutron porosity log (v/v) |
| $RHOB$ | Density log (gm/cm3) |
| $SSAU$ | Seminole San Andres Unit |

## Nomenclature

| | |
|---|---|
| $\lVert \ \rVert_2$ | L2 norm, mean squared error |
| $\mathcal{L}_{adv_D}$ | Discriminator adversarial loss |
| $\mathcal{L}_{adv_G}$ | Generator adversarial loss |
| $\mathcal{L}_{adv_{GC}}$ | Generator adversarial loss when the well log uncertainty is known |
| $\mathcal{L}_{lc}$ | Linear constraint |
| $\mathcal{L}_{linear}$ | Loss of linear model |
| $\mathcal{L}_{pred}$ | Prediction error of training (validation) set |
| $C_d$ | Formation property prediction covariance matrix |
| $\tilde{X}$ | Preprocessed predictor features (normalized well logs) |

| | |
|---|---|
| $\tilde{Y}$ | Response feature prediction (petrophysical property, permeability prediction) |
| $\bar{Y}$ | Average value of the formation property of well(s) |
| $A, B$ | Coefficients of a linear model |
| $Cov$ | Covariance calculation |
| $D$ | Discriminator |
| $E$ | Prediction difference of different models |
| $G$ | Generator |
| $M$ | Mapping layers |
| $P$ | Preprocessing layers |
| $X$ | Predictor features (well logs) |
| $Y$ | Response features (petrophysical properties, permeability) |
| $x, y, \tilde{x}, \tilde{y}$ | Samples drawn from data set of corresponding features |
| $\mathbb{E}$ | Expectation |
| $\lambda$ | Certainty of unbiased well logs in the test set |

## Subscripts & Suffix

| | |
|---|---|
| $\_DA$ | Normalized well logs and permeability prediction calculated with the DA model |
| $\_linear$ | Normalized well logs and permeability prediction calculated with the linearly constrained model |
| $\_origin$ | Original well logs and permeability prediction calculated with the model without any constraints |
| $\_scaling$ | Normalized well logs and permeability prediction calculated with two-point scaling method |
| $l$ | Linear model |
| $s$ | Features/Layers from training set |
| $t$ | Features/Layers from test set |
| $u$ | Unbiased measurements |

## Acknowledgements

# References

Bennis, M., and C. Torres-Verdín, 2019, Estimation of dynamic formation properties from multiple well logs using machine learning and unsupervised rock classification: Presented at the SPWLA 60th Annual Logging Symposium, Society of Petrophysicists and Well Log Analysts.

Bestagini, P., V. Lipari, and S. Tubaro, 2017, A machine learning approach to facies classification using well logs: Technical Program, Society of Exploration Geophysicists, Expanded Abstracts, 2137-2142.

Bhattacharya, S., and S. Mishra, 2018, Applications of machine learning for facies and fracture prediction using Bayesian network theory and random forest: case studies from the Appalachian Basin, USA: Journal of Petroleum Science and Engineering, **170**, 1005-1017.

Borg, I., and P. J. Groenen, 2005, Modern multidimensional scaling: theory and applications: Springer Science & Business Media.

Brazell, S., A. Bayeh, M. Ashby, and D. Burton, 2019, A machine-learning-based approach to assistive well-log correlation: Petrophysics, **60**, 469-479.

Chang, J., J. Li, Y. Kang, W. Lv, T. Xu, Z. Li, W. X. Zheng, H. Han, and H. Liu, 2021, Unsupervised domain adaptation using maximum mean discrepancy optimization for lithology identification: Geophysics, **86**, ID19-ID30.

Collobert, R., and J. Weston, 2008, A unified architecture for natural language processing: deep neural networks with multitask learning: 25th International Conference on Machine Learning, International Conference on Machine Learning, proceedings, 160–167. doi:10.1145/1390156.1390177.

Gaillot, P., J. Lewandowski, and R. Nursaidova, 2019, Uncertainty analysis in formation evaluation: rationale, methods and examples: Presented at SPWLA 60th Annual Logging Symposium, Society of Petrophysicists and Well Log Analysts.

Gashler, M., 2008, Decision tree ensemble: small heterogeneous is better than large homogeneous: Seventh International Conference on Machine Learning and Applications,

International Conference on Machine Learning, proceedings, 900–905. doi:10.1109/ICMLA.2008.154

Goodfellow, I., J. Pouget-Abadie, M. Mirza, B. Xu, D. Warde-Farley, S. Ozair, A. Courville, and Y. Bengio, 2014, Generative adversarial nets: Advances in neural information processing systems, 27.

Greder, H. N., P. Y. Diver, S. Danquigny, and F. M. Pellerin, 1996, Determination of permeability distribution at log scale in vuggy carbonates: Presented at the SPWLA 37th Annual Logging Symposium, Society of Petrophysicists and Well Log Analysts.

Jo, H., W. Pan, J. E. Santos, H. Jung, and M. J. Pyrcz, 2021, Machine learning assisted history matching for a deepwater lobe system: Journal of Petroleum Science and Engineering, **207**, 109086.

Kullback, S., and R. A. Leibler, 1951, On information and sufficiency: Annals of Mathematical Statistics, **22** (1), 79–86. doi:10.1214/aoms/1177729694.

Leverett, M., 1941, Capillary behavior in porous solids: Transactions of the AIME, **142**(01), 152-169. https://doi.org/10.2118/941152-G

Liang, L., T. Le, T. Zimmermann, S. Zeroug, and D. Heliot, 2019, A machine learning framework for automating well log depth matching: Presented at the SPWLA 60th Annual Logging Symposium, Society of Petrophysicists and Well Log Analysts.

Male, F., and I. J. Duncan, 2020, Lessons for machine learning from the analysis of porosity-permeability transforms for carbonate reservoirs: Journal of Petroleum Science and Engineering, **187**, 106825. https://doi.org/10.1016/j.petrol.2019.106825

Mallan, R. K., J. Thorne, P. Rice, E. Toumelin, J. B. Clavaud, and B. Bilodeau, 2018, Petrophysical uncertainty analysis using spatial bootstrapping: Presented at the SPWLA 59th Annual Logging Symposium, Society of Petrophysicists and Well Log Analysts.

Manning, C. D., and H. Schutze, 1999, Foundations of statistical natural language processing: MIT Press.

Mohaghegh, S., B. Balan, and S. Ameri, 1997, Permeability determination from well log data: SPE Formation Evaluation, **12**(03), 170-174. https://doi.org/10.2118/30978-PA

Pan, W., C. Torres-Verdín, and M.J. Pyrcz, 2021, Stochastic Pix2pix: a new machine learning method for geophysical and well conditioning of rule-based channel reservoir models: Natural Resource Research, **30**, 1319–1345. https://doi.org/10.1007/s11053-020-09778-1

Pérez-Cruz, F., 2008, Kullback-Leibler divergence estimation of continuous distributions: 2008 IEEE International Symposium on Information Theory, Institute of Electrical and Electronics Engineers, Proceedings, 1666-1670.

Prasad, M., C. Olsen, and I. Fabricius, 2004, Rock physics and statistical well log analyses in carbonates: Presented at Annual Meeting, Society of Exploration Geophysicists.

Pyrcz, M. J., and C. V. Deutsch, 2014, Geostatistical reservoir modeling: Oxford University Press.

Santos, J.E., Y. Yin, H. Jo, W. Pan, Q. Kang, H. S. Viswanathan, M. Prodanović, M. J. Pyrcz, N. Lubbers, 2021, Computationally efficient multiscale neural networks applied to fluid flow in complex 3D porous media: Transport in Porous Media, **140**, 241–272. https://doi.org/10.1007/s11242-021-01617-y

Sasaki, H., Y. K. Noh, and M. Sugiyama, 2015, Direct density-derivative estimation and its application in KL-divergence approximation: International Conference on Artificial Intelligence and Statistics, Machine Learning Research, Proceedings, 809-818.

Shao, W., S. Chen, M. Eid, and G. Hursan, 2019, Carbonate log interpretation models based on machine learning techniques: Presented at the 60th Annual Logging Symposium, Society of Petrophysicists and Well Log Analysts.

Shashank, S., and M. P. Mahapatra, 2018, Boosting rock facies prediction: weighted ensemble of machine learning classifiers: Presented at the Abu Dhabi International Petroleum Exhibition & Conference, SPE. https://doi.org/10.2118/192930-MS

Shier, D. E., 2004, Well log normalization: methods and guidelines, Petrophysics, **45**(03), 268-280.

Sidahmed, M., A. Roy, and A. Sayed, 2017, Streamline rock facies classification with deep learning cognitive process: presented at the SPE Annual Technical Conference and Exhibition, SPE. doi:10.2118/187436-MS

Timur, A., 1968, An investigation of permeability, porosity, and residual water saturation relationships for sandstone reservoirs: The Log Analyst, **9** (4), P8.

Tzeng, E., J. Hoffman, K. Saenko, and T. Darrell, 2017, Adversarial discriminative domain adaptation: IEEE Conference on Computer Vision and Pattern Recognition, Institute of Electrical and Electronics Engineers, Proceedings, 7167-7176.

Wang, F. P., F. J. Lucia, and C. Kerans, 1998, Integrated reservoir characterization study of a carbonate ramp reservoir: Seminole San Andres Unit, Gaines County, Texas, SPE Reservoir Evaluation and Engineering, 105–113. doi:10.2118/36515-PA

Wang, Q., S. R. Kulkarni, and S. Verdú, 2009, Divergence estimation for multidimensional densities via k-nearest-neighbor distances: IEEE Transactions on Information Theory, **55**(5), 2392-2405.

Xu, W., T.T. Tran, R.M. Srivastava, 1992, Integrating seismic data in reservoir modeling: the collocated Cokriging alternative: Presented at the SPE Annual Technical Conference and Exhibition, SPE. http://dx.doi.org/10.2118/24742-MS

Yu, Y., C. Xu, S. Misra, W. Li, M. Ashby, W. Pan, T. Deng, H. Jo, J. E. Santos, 2021, Synthetic sonic log generation with machine learning: a contest summary from five methods: Petrophysics, **62**, 393–406. doi: https://doi.org/10.30632/PJV62N4-2021a4

Zhong, Z., T. R. Carr, X. Wu, and G. Wang, 2019, Application of a convolutional neural network in permeability prediction: a case study in the Jacksonburg-Stringtown oil field, West Virginia, USA: Geophysics, **84**(6), 363-373. https://doi.org/10.1190/geo2018-0588.1

Zhu, L., H. Li, Z. Yang, C. Li, and Y. Ao, 2018, Intelligent logging lithological interpretation with convolution neural networks: Petrophysics, **59**, 799–810. doi: https://doi.org/10.30632/PJV59N6-2018a5